npj | climate and atmospheric science

www.nature.com/npjclimatsci

ARTICLE OPEN

Check for updates

# Impact of tropical SSTs on the late-winter signal over the North Atlantic-European region and contribution of midlatitude Atlantic

Ivana Herceg-Bulić[1]✉, Sara Ivasić[1] and Margareta Popović[1]

The impact of tropical sea surface temperatures (SSTs) on the signal of geopotential heights (GH200) over the North Atlantic-European (NAE) region is analysed from the aspects of seasonality, the contribution of individual tropical basins and midlatitude North Atlantic, El Niño-Southern Oscillation (ENSO) effect and spatial pattern of the atmospheric response. For this purpose, ensembles of targeted numerical simulations with SST forcing prescribed in various ocean basins are performed and examined. A clear atmospheric response is obtained in the late winter months. The strongest signal is linked to ENSO events during late winter. The competitive influences of individual tropical basins are indicated. At the same time, the superposition effect of the extratropical North Atlantic SSTs, which is established through the modulation of storm tracks, is demonstrated. Both, the modelled signal and the NOAA-CIRES-DOE 20th Century Reanalysis variance reveal the ENSO signature as a pattern in the North Atlantic projecting onto the East Atlantic pattern.

*npj Climate and Atmospheric Science* (2023)6:172 ; https://doi.org/10.1038/s41612-023-00493-1

## INTRODUCTION

Sea surface temperatures (SSTs) in the tropics can act as a source of boundary-forced predictability for the atmosphere in the extratropics, characterised by large internal variability and poor predictability. Among the strongest events with such an influence on climate variability worldwide is the El Niño-Southern Oscillation (ENSO). ENSO impacts climate variability from seasonal to interannual time scales through tropospheric and stratospheric pathways (e.g. refs. [1–5]). While the ENSO teleconnection towards the Pacific North American region is well-researched and understood, there are still many processes that blur the ENSO signature over the North Atlantic-European region (NAE). For example, there are differences between early and late winter ENSO impact on the NAE region[6–10]. Furthermore, many papers show that the late wintertime ENSO signature over the NAE region resembles the pattern of the North Atlantic Oscillation (NAO) (e.g.[11–13],). At the same time, the NAO itself also accounts for the highest amount of climate variability[14]. Furthermore, as an internal mode of variability, NAO appears as noise in AGCM simulations[15] (hereafter IHB2023[15]). Examining the Pacific North American region, Lopez and Kirtman[16] found that the ENSO-forced response is highly influenced by atmospheric internal variability, which can be up to ten times larger in amplitude.

In addition to the tropical Pacific, other oceans also affect the NAE region. Therefore, the influence from other basins can interfere with ENSO's impact and modulate its signature over the NAE region. For example, the Indian Ocean has a significant influence on the NAE response to ENSO during the early winter season[6,8]. Nevertheless, the Atlantic is the closest to our area of interest and has an impact on the NAE climate variability[17–19]. In addition to its regional influence on the NAE region, the Atlantic can also actively contribute to the NAE ENSO atmospheric signal. Through the so-called atmospheric bridge[20–22], ENSO-related SST anomalies generate a midlatitude SST response in the North Atlantic. That SST pattern reinforces the atmospheric flow that has driven it, enabling a more persistent ENSO signal over the NAE region[23,24]. ENSO also affects the midlatitude cyclone activity which is manifested as a shift in storm tracks. During El Niño, the North Pacific storm track is shifted equatorward and extended eastward toward the North Atlantic region linking the Pacific and Atlantic storm tracks (e.g. refs. [25,26],). Through the interaction with large-scale atmospheric circulation, storm tracks considerably contribute to the momentum, moisture and poleward heat transports. There are many factors influencing the intensity and position of storm tracks, among them the SST distribution[27,28]. For example, a warm sea surface acts as a source of heat and moisture that supports cyclone development. Thus, the SST pattern in the extratropical Atlantic that has been driven by ENSO through the 'atmospheric bridge' can also exert a local effect on the Atlantic storm tracks. Therefore, a two-way atmosphere-ocean coupling via storm tracks is possible in the extratropical North Atlantic, as well as a modification of the ENSO signature there.

Recently, IHB2023[15] analysed the late-winter variability and predictable components of geopotential heights (GH200) over the NAE region based on modelling experiments with SSTs prescribed in different parts of tropical oceans. They demonstrated that the interannual variability of the pattern with the strongest signal-to-noise ratio (optimal pattern) is correlated with tropical SSTs. They also report the similarity between the first empirical orthogonal pattern (EOF1) of the ensemble mean and the optimal pattern, implying that EOF1 of the ensemble mean reflects a potentially predictable signal. Relying on the results of IHB2023[15] and existing knowledge of the ENSO-NAE teleconnection, this paper examines the influence of tropical oceans on the variability of the NAE region from the following hitherto unexplored aspects: subseasonal evolution of the GH200 signal, contribution of individual tropical basins, ENSO and non-ENSO signal, spatial pattern of the signal, two-way ocean-atmosphere interaction in the extratropical North Atlantic via storm tracks and its modification of the atmospheric response to ENSO.

[1]Department of Geophysics, Faculty of Science, University of Zagreb, Zagreb, Croatia. ✉email: ivana.herceg.bulic@gfz.hr

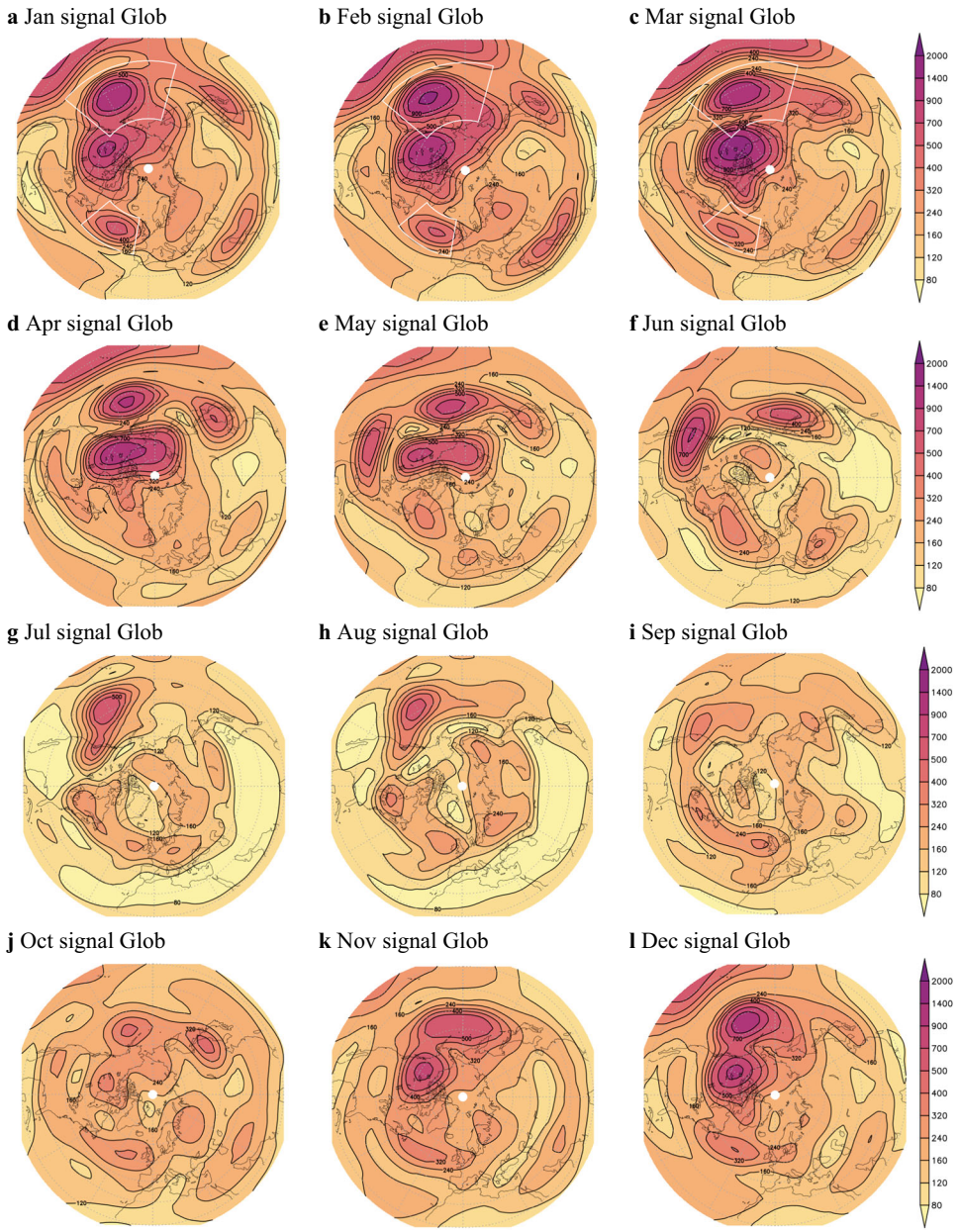


**Fig. 1 Monthly signal of geopotential heights at 200 hPa [m$^2$]. a–l** Signal for the whole 156-year period in ICTP AGCM Glob experiment. White contours in (**a**–**c**) highlight the NAE max (40°–60° N, 50°–10° W) and PNA max (30°–60° N, 165° E–130° W) areas.

## RESULTS

### Seasonality of GH200 signal

The monthly GH200 signal in the ICTP AGCM forced with global SST anomalies (SSTA; Glob; Supplementary Fig. 1a) is depicted in Fig. 1. The strongest signal (in terms of amplitude and spatial extension) appears over the North Pacific and is particularly strong in the late-winter season (January, February, and March; Fig. 1a–c). A secondary signal maximum occurs over the North Atlantic. Both, Pacific and Atlantic maximums, have similar seasonality – the strengthening of the signal starts in late autumn (October; Fig. 1j) and continues to gradually increase until winter when it reaches its maximum (January and February, Fig. 1a, b). The rest of the AGCM experiments show a similar seasonal development of the signal over the Pacific and Atlantic with a maximum in late winter (Supplementary Fig. 2; only the late-winter season is shown). The response in the experiments involving SST forcing in the tropical Pacific (TroPac and Tropics; Supplementary Fig 2j–o) is similar to that in Glob (Fig. 1a–c). The experiment with no SST forcing (Clim, Supplementary Fig. 2p–r), and the experiments with SST forcing prescribed in the tropical Atlantic and tropical Indian Ocean (TroAtl and TroInd; Supplementary Fig. 2d–i) have a very weak signal amplitude. The signal obtained in the Clim experiment, an experiment with no SST forcing, should be considered as a numerical residual that is associated with internal atmospheric variability. Each simulation within the Clim ensemble differs slightly by the imposed initial conditions. Therefore, in a finite ensemble, the Clim ensemble mean is not identical to its climatological mean, and, as a result, a weak signal is obtained. Since the signal in the other SST-forced experiments (Supplementary Fig. 2a–o) consists of the forced component and internal atmospheric variability, the Clim signal can be used as a measure

of significance for the rest of the experiments. Namely, when the SST-forced signal is greater than the Clim signal, it indicates that the forced component exceeds atmospheric internal variability, and thus can be considered significant.

### ENSO and non-ENSO signal

Analysis of SST sensitivity experiments indicates that the tropical Pacific is a key factor in achieving a pronounced extratropical signal during winter. Given that ENSO is the most prominent mode of SST variability in the tropical Pacific, we examine its contribution to the extratropical GH200 signal focusing on late winter. We categorise the data into ENSO and non-ENSO years, as described in the "Methods" section, and calculate the signal for each category. The ENSO-related signal (Fig. 2) reveals two prominent centres in the Pacific North American (PNA) region in the Glob, TroPac, and Tropics experiments, while their amplitudes are less pronounced in the TroInd experiment (Fig. 2). Meanwhile, the TroAtl and Clim experiments are mutually comparable but feature a smaller amplitude of the signal compared to the rest of the experiments.

In addition to the PNA, there is also a detectable signal over the NAE region. Similar to the signal in Fig. 1, the ENSO-related NAE signal in the Glob (Fig. 2a–c) has a predominantly monopolar pattern over the Atlantic Ocean. The greatest amplitude is found in February and March in the TroPac experiment (Fig. 2k, l). Generally, the TroPac experiment has a spatial pattern similar to that of the Glob signal. However, as we expand the area of the prescribed boundary forcing to the whole tropical zone, the signal weakens but spatially stays similar (Tropics; Fig. 2m–o). Compared to the rest of the experiments, the TroAtl, TroInd, and Clim ENSO signals are weaker (Fig. 2d–i, p–r). Extracting only ENSO years yields a stronger signal over the NAE region in the Glob, TroPac and Tropics experiments (cf. Fig. 2 with Supplementary Fig. 2).

The late-winter signal calculated only for non-ENSO years is presented in Fig. 3. Overall, the non-ENSO signal is weaker than the signal for both ENSO years and the entire considered period. The non-ENSO signal is the strongest in the Glob experiment (Fig. 3a–c). However, it is mostly weak (≤200 $m^2$) outside of the PNA region in the rest of the experiments. Over the NAE region, in the Glob (Fig. 3a–c) and Tropics (Fig. 3m–o) experiments, the non-ENSO signal retains the monopolar shape similar to the signal calculated for all years (Supplementary Fig. 2) and ENSO years (Fig. 2). Similarly, the TroAtl (Fig. 3d–f) and TroPac (Fig. 3j–l) experiments display a predominantly zonal signal shape with a smaller amplitude. The TroInd signal has a weak centre in January (Fig. 3g), while the signal in both February and March (Fig. 3h, i) is more zonally extended across the NAE region.

### Signal averaged over the PNA and NAE region

Returning to our area of interest, the centre over the North Atlantic was identified as the most prominent feature of the NAE signal in the late-winter season (40°−60° N, 50°−10° W; Figs. 1–3). Therefore, in this section, we averaged the monthly GH200 signal over this NAE maximum (NAE max; white contours in Fig. 1a–c) and the whole available period, ENSO and non-ENSO years, respectively (Fig. 4). The amplitude of this averaged signal for all years (Fig. 4a) is the highest in the late-winter months (January–March). The signal starts to decrease until June, when the amplitude reaches a summer maximum, immediately followed by a minimum in July. The NAE max signal gradually increases from August until December, when the amplitude becomes comparable to the late-winter months.

The spatially averaged signal in ENSO years (Fig. 4b) has higher values for all experiments in February, which is indicated by the ratio of the ENSO signal and the signal for all years shown above each column. The largest increase in the ENSO signal compared to the signal for the entire period is in March for the TroPac experiment (52%). Considering February and March together, the strongest ENSO-related signal is obtained in the TroPac experiment, followed by Glob and Tropics. A significant increase in the TroPac signal is also recorded in June (45%), indicating a possible presence of the delayed influence of ENSO events on the NAE region[24], although it may also be related to some other tropical SST influences (e.g., response to summertime ENSO[29]). Meanwhile, the non-ENSO signal (Fig. 4c) is comparable in amplitude to the signal for all years (Fig. 4a), indicated by the ratio of the non-ENSO signal and the signal- for all years displayed above each column.

Inspection of the Northern Hemisphere signal (Figs. 1–3) showed that the PNA features the highest values of signal on the hemispheric scale. Following Chapman et al.[30], we calculated the GH200 signal average over the maximum in the PNA region (30°−60° N, 165° E to 130° W; white contours in Fig. 1a–c). This signal averaged over the PNA maximum (Fig. 4d–f) shows a clear seasonal behaviour, with the highest amplitude in winter which gradually decreases through the spring and summer seasons. Generally, the signal for all years (Fig. 4d) is the strongest in the Glob experiment. On the other hand, the TroAtl signal is consistently the smallest across all months compared to the rest of the SST-forced experiments. The signal amplitude in the TroPac and Tropics experiments is smaller than in the Glob experiment. The ENSO signal averaged over the PNA region has similar characteristics – winter maximum and a prolonged summer-autumn minimum (July–October; Fig. 4e). However, the differences between the high winter and lower late summer/early autumn amplitudes of the signal variance are more pronounced in ENSO years than for all years (cf. Fig. 4d, e). Simultaneously, the non-ENSO signal (Fig. 4f) is generally smaller than the signal in all years and ENSO years, while the differences between the amplitude of the signal in summer and winter are not as pronounced.

Referring to the presented results, which confirmed that the strongest extratropical response to ENSO is during late winter, we focus on this season (January, February, and March). Here, we examine the dependence of the signal with respect to the origin of tropical SST forcing. We first check the linearity of the response to the forcing from different parts of the tropical ocean by comparing the sum of the signals obtained in TroPac, TroInd, and TroAtl with the signal in the Tropics. According to Fig. 5, over both PNA and NAE regions, the sum of the TroPac, TroAtl and TroInd signals projects on the same pattern as the signal in the Tropics experiment, but with weaker amplitude. Previous results have already shown that, in general, the TroPac signal is stronger compared to the Tropics signal, which may indicate a competing influence of certain parts of the tropical ocean. The extratropical response reveals a nonlinearity of amplitude with respect to the origin of the tropical forcing but is simultaneously anchored in terms of the spatial pattern of the signal.

### ENSO signature in reanalysis data

Sensitivity AGCM experiments show a noticeable influence of the tropical Pacific (ENSO) on the GH200 signal, not only in the PNA but also in the NAE area. Here, we use the NOAA-CIRES-DOE 20th Century Reanalysis V3[31] (hereafter 20CRV3) in the same 156-year period as our AGCM simulations to check whether we can detect an ENSO footprint in that dataset as well. Since the reanalysis consists of only one realisation, the signal cannot be calculated in the same way as for the AGCM simulations using Eq. (1). Instead, the variance of the 20CRV3 geopotential heights at 200 hPa was used and qualitatively compared with the modelled signal. For the sake of comparability with the signal based on Eq. (1), and to exclude internal atmospheric variability, we included only the ENSO and non-ENSO years when the NAO conditions were neutral (i.e., $-0.5\ \sigma < \text{NAO index} < +0.5\ \sigma$) in the calculation of the variance. To classify the data into the (non)ENSO and NAO-neutral

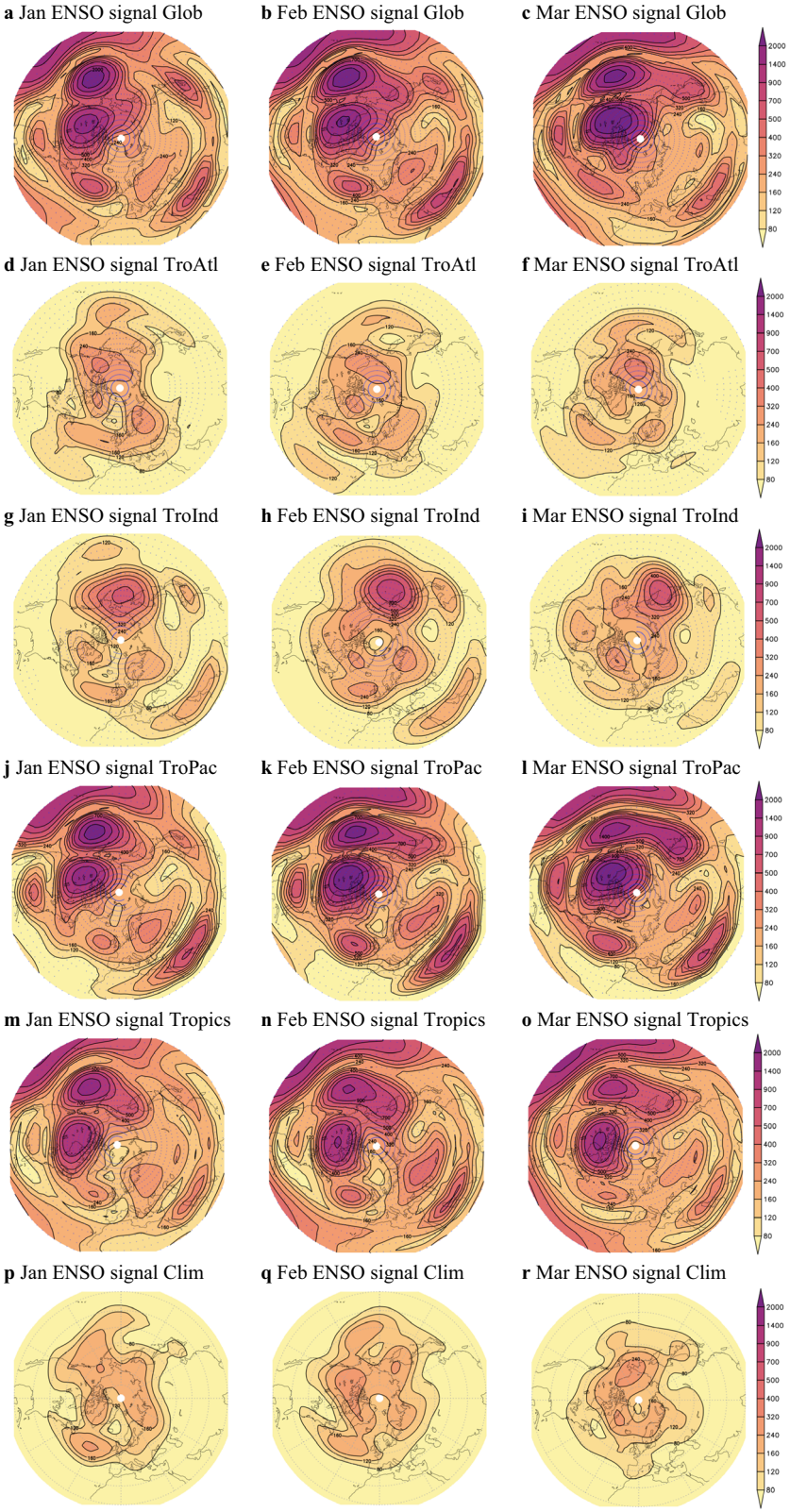


**Fig. 2 Signal of geopotential heights at 200 hPa [$m^2$] in the 53 ENSO years in January (left), February (middle), and March (right) in the ICTP AGCM experiments. a–c** Glob, **d–f** TroAtl, **g–i** TroInd, **j–l** TroPac, **m–o** Tropics, and **p–r** Clim. The 53 ENSO years were selected from the 156 years according to the strength of the Niño3.4 index in the JFM season ($|N3.4| > 1\sigma$) based on NOAA ERSST V3 SST anomalies. Blue dots in (**a–o**) indicate centres of gridboxes with values larger than the Clim ENSO signal.

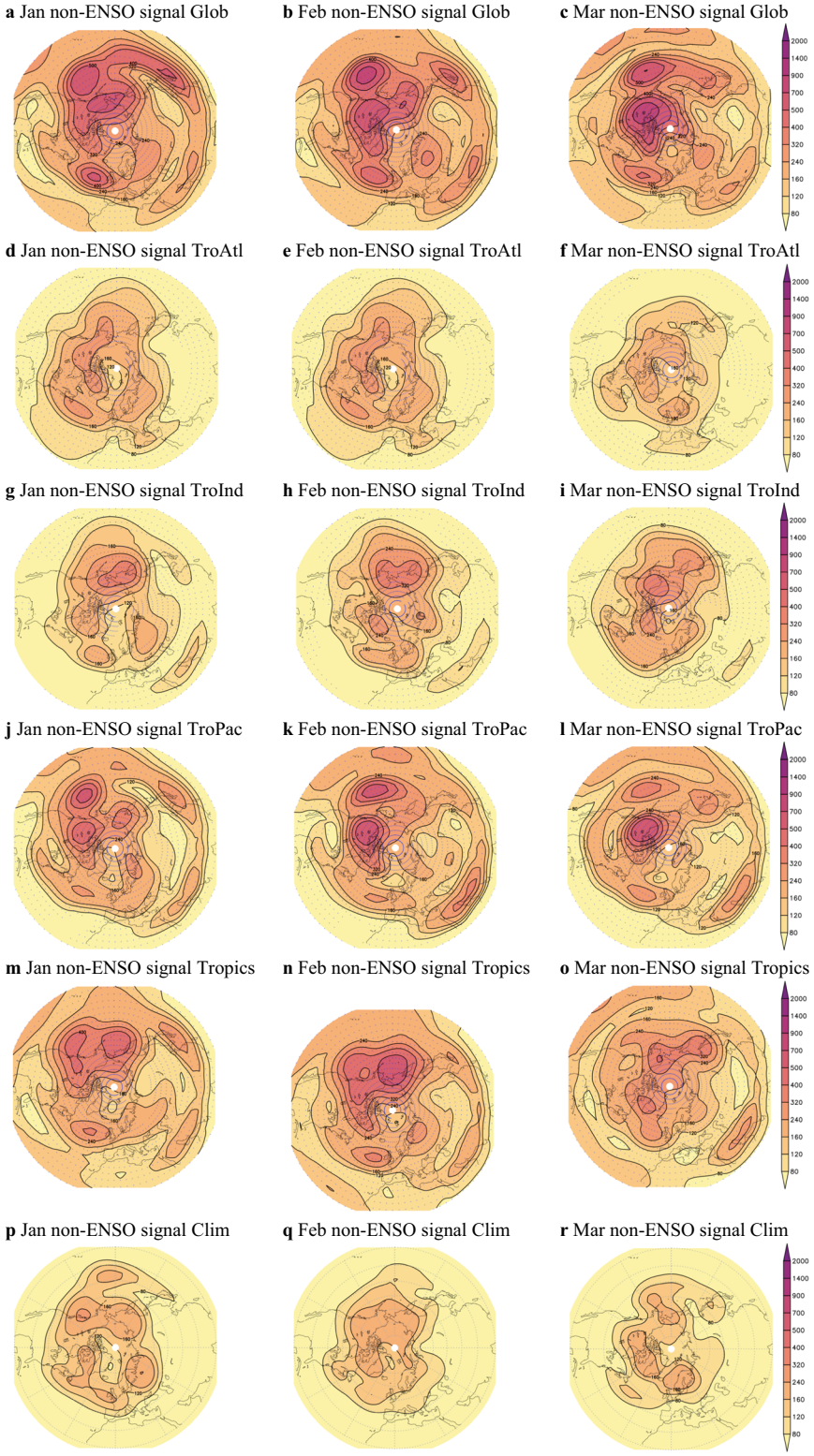


**Fig. 3 Signal of geopotential heights at 200 hPa [m$^2$] in the 57 non-ENSO years in January (left), February (middle), and March (right) in the ICTP AGCM experiments. a–c** Glob, **d–f** TroAtl, **g–i** TroInd, **j–l** TroPac, **m–o** Tropics, and **p–r** Clim. The 57 non-ENSO years were selected from 156 years according to the strength of the Niño3.4 index in the JFM season ($-0.5\ \sigma < |N3.4| < 0.5\ \sigma$) based on NOAA ERSST V3 SST anomalies. Blue dots in (**a–o**) indicate centres of gridboxes with values larger than the Clim non-ENSO signal.

categories, we use the JFM Niño3.4 and NAO index based on 20CRV3 SSTA and sea level pressure data. According to the 20CRV3 data, there are 50 NAO-neutral years in the whole 156-year period. Of those 50, 13 are also considered ENSO years, while 21 years are simultaneously sorted as non-ENSO and NAO-neutral. January variance (Fig. 6a) is characterised by five local maximums spread across the Northern Hemisphere around 50° N. In February (Fig. 6b), the most prominent feature of the GH200 variance is a

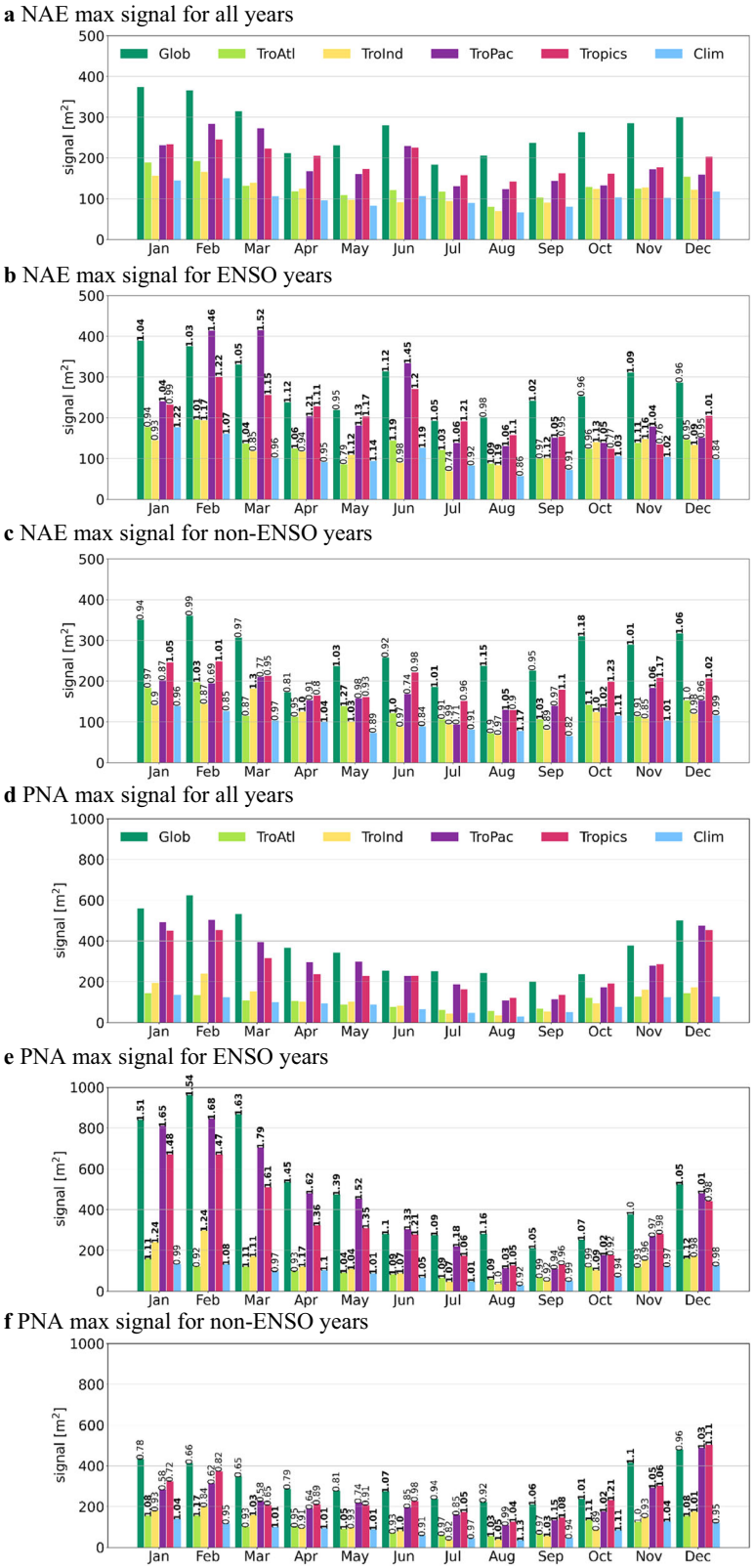


**Fig. 4 Monthly signal of geopotential heights at 200 hPa [m$^2$] in the ICTP AGCM experiments (Glob, TroAtl, TroInd TroPac, Tropics and Clim) averaged over the maximum in the North Atlantic (NAE max; 40°–60° N, 50°–10° W) and in the Pacific North American region (PNA max; 30°–60° N, 165° E–130° W).** NAE max signal for **a** all years (156), **b** ENSO years (53), and **c** non-ENSO years (57). PNA max signal for **d** all years (156), **e** ENSO years (53), and **f** non-ENSO years (57). The number above each column in (**b**, **c**, **e**, **f**) is the ratio of the ENSO (non-ENSO) signal and signal for all years.

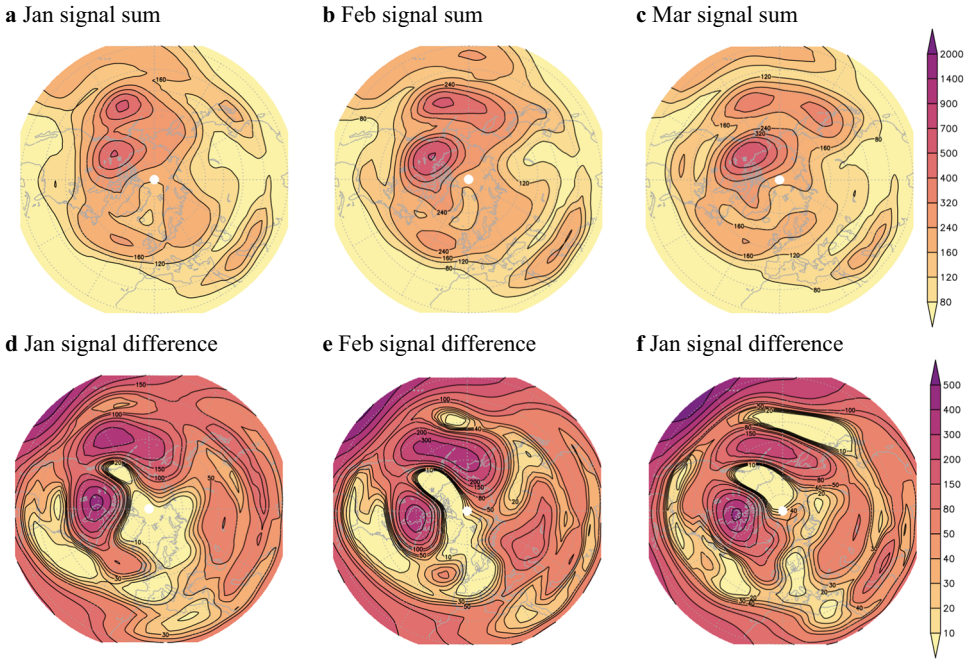


**Fig. 5 Sum of the signal of geopotential heights at 200 hPa [m$^2$] in the TroAtl, TroPac and TroInd ICTP AGCM experiments. a** January, **b** February, and **c** March. The difference between the Tropics signal and sum of the TroAtl, TroPac and TroInd signal for **d** January, **e** February, and **f** March.

centre south of Greenland. Going into March (Fig. 6c), the 20CRV3 variance has two action centres—in the location of the Aleutian Low and between Greenland and North America, roughly at the same latitude. There is also a weak centre located over the UK in March.

In ENSO years during NAO-neutral conditions (Fig. 6d–f), the spatial configuration of the variance stays the same as the variance for all NAO-neutral years. However, the variance amplitude is increased in all local maximums compared to the variance for all NAO-neutral years.

The GH200 variance for the non-ENSO and NAO-neutral years (Fig. 6g–i) shares the main spatial characteristics with the other two categories. In January (Fig. 6g), only the amplitude of the centre above the North Atlantic and northwest of Greenland remains comparable to the NAO-neutral counterpart (Fig. 6a), while the rest of the local maximums are weakened. There is also an additional centre over the Atlantic (~30° N, 30° W). In February (Fig. 6h), the non-ENSO variance has a higher amplitude over Northern Europe, southwestern Greenland, and the eastern coast of North America compared to the NAO-neutral variance (Fig. 6b). Finally, the March non-ENSO variance (Fig. 6i) has a more pronounced maximum over Northern Europe in comparison to its NAO-neutral counterpart (Fig. 6c). It is obvious that the ENSO variance (especially in January and February, Fig. 6d, e) resembles the modelled ENSO signal over the NAE region (Fig. 2a, b). In general, classification into ENSO and non-ENSO events affects associated variance fields. The main feature of the GH200 variance related to ENSO events is the pattern that persists in the late-winter season, having a stronger amplitude over the North Atlantic and North Pacific than for non-ENSO events.

### Impact of the extratropical North Atlantic on the NAE ENSO-related signal

Both NAE and PNA signals are excited by ENSO and have a maximum in late winter. However, there are some remarkable differences between them. First, the NAE signal is weaker than the PNA signal. The differences between ENSO and non-ENSO signals are smaller when averaged over the NAE region. Also, analysis of the NAE signal in different experiments indicates a destructive interference of the tropical ocean influences and possible amplifying contribution of the North Atlantic. Thus, the NAE ENSO signal (Fig. 4b) showed that the signal obtained in the Tropics experiment is weaker than its TroPac counterpart, indicating a partial cancellation between the influence of different parts of tropical oceans. On the other hand, the Glob NAE signal is stronger than both TroPac and Tropics in January and is stronger than Tropics in February and March, suggesting a possible amplifying influence of extratropical oceans. To test this assumption, we have run an additional ensemble of numerical simulations in the same manner as the other experiments, but with SST forcing prescribed everywhere except in the extratropical North Atlantic (NoNAtl; Supplementary Fig. 1f) and with SST forcing kept only in extratropical North Atlantic (Natl; Supplementary Fig. 1g). The idea of the NoNAtl experiment is to keep the SST forcing in all parts of the ocean (including the influence of ENSO) but to omit the extratropical North Atlantic and thus eliminate its possible influence. Compared to the Glob experiment (Fig. 1a–c), the NoNAtl signal (Fig. 7a–c) has the same spatial distribution with no change in the positions of the action centres. Furthermore, the ENSO signal (Fig. 8d–f) is stronger than the signal based on all simulated years (Fig. 7a–c). The consideration of only ENSO-related signal results in a stronger response in the NAE region that manifests itself as a prominent monopole over the North Atlantic. The comparison of ENSO Glob (Fig. 2a–c) and ENSO NoNAtl signals (Fig. 7d–f) shows that the same spatial response field occurs in both experiments, and this is because the main source of the signal (tropical Pacific, i.e., ENSO) is present in both experiments. Nevertheless, the comparison of response amplitudes implies a positive contribution from the North Atlantic, as it is considerably larger for the ENSO Globe experiment (36% and 20% in January and February, respectively).

To further examine the contribution of the North Atlantic, experiment NAatl was performed with SST forcing limited only to the midlatitude Atlantic (Fig. 8). Although weaker in amplitude, a

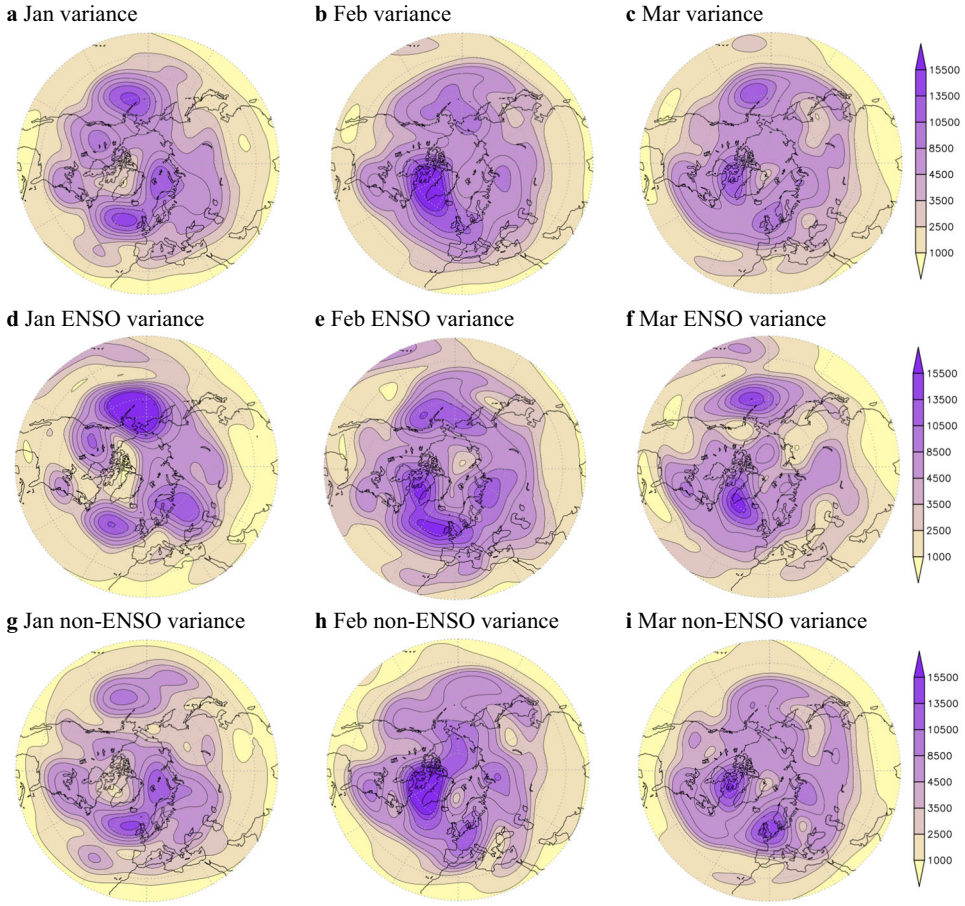


**Fig. 6 January, February, and March variance of geopotential heights at 200 hPa [m$^2$] in the NOAA-CIRES-DOE 20th Century Reanalysis V3 dataset. a–c** all NAO neutral years (50), **d**, **e** ENSO strong NAO neutral years (13), and **g–i** non-ENSO NAO neutral years (21). ENSO events are classified according to the strength of the JFM NOAA Niño3.4 index ($N3.4 > 1\sigma$ or $N3.4 < -1\sigma$). NAO neutral years are defined according to the strength of the JFM NAO index ($-0.5\sigma <$ NAO index $< 0.5\sigma$).

signal over the North Atlantic can be observed here as well, which has the same shape as the one in the Glob experiment, especially for January and February (cf. Fig. 1a–c and Fig. 8a–c). Furthermore, the Natl ENSO signal (Fig. 8d–f) over the North Atlantic is similar in both shape and amount of the total signal (Fig. 1d–f), while it disappears for non-ENSO events (Fig. 8g–i). This shows that the total signal is dominantly related to ENSO. Although the NAtl experiment contains no forcing in the tropical Pacific, and therefore neither ENSO, its influence is indirectly present in the Atlantic SST anomalies. Namely, observed SSTs were imposed as a lower boundary forcing in the experiment and they are the result of all processes in nature, thus, ENSO as well. Consequently, measured SSTs in the extratropical North Atlantic also reflect the influence of the tropical Pacific on the Atlantic that has been established through the atmospheric bridge. From this point of view, the categorisation into ENSO and non-ENSO events is justified, as well as the discussion of the influence of Atlantic SSTs on the ENSO signal over the NAE area.

### Storm track response to ENSO and the role of extratropical North Atlantic SSTs

The NoNAtl and NAtl experiments indicated the contribution of the midlatitude North Atlantic to the NAE ENSO signal. The North Atlantic can support the persistence of certain atmospheric signals such as ENSO and NAO. In the case of ENSO, tropical Pacific SSTs drive Atlantic SSTs through the 'atmospheric bridge'. Generated anomalous SST field reinforcing the atmospheric circulation that has generated it[32]. Furthermore, cyclonic development is sensitive to the structure of the SST field, and therefore the ENSO-induced SST anomaly field in the North Atlantic can have a local influence on cyclones. Here, we focus on the atmosphere-ocean coupling via Atlantic storm tracks as a mechanism of the local SST impact on the ENSO signal. To analyse the modelled ENSO impact on storm activity, we used the variance (for periods of 1–30 days) of the geopotential height at 500 hPa (VarGH500) and presented it as composites of the El Niño-La Niña difference.

The amplitude of the monthly climatology means of VarGH500 shows two maxima associated with the Pacific and Atlantic storm tracks (Fig. 9, contours). There is no significant difference in their position and amplitude between the Glob and NoNAtl experiments. More significant differences are depicted in the VarGH500 composites for ENSO events (Fig. 9, shading). There, the Glob experiment clearly shows the equatorward shift of storm activity during El Niño events (Fig. 9a–c). A seasonal development is found with the strengthening of storm activity over the North Atlantic from January to March. This result is consistent with existing literature (e.g. ref. [26]) and shows that, once the teleconnection between the tropical Pacific and the NAE region is established via Rossby waves, an impact on storm activity and poleward heat transport is realised. Over the North Atlantic, in the TroAtl experiment (not shown) there is a weak influence on the VarGH500 consistent with the Glob experiment, indicating an indirect ENSO influence via the Atlantic Ocean.

Given that the previous results pointed to the NoNatl experiment as an indicator of the influence of the extratropical

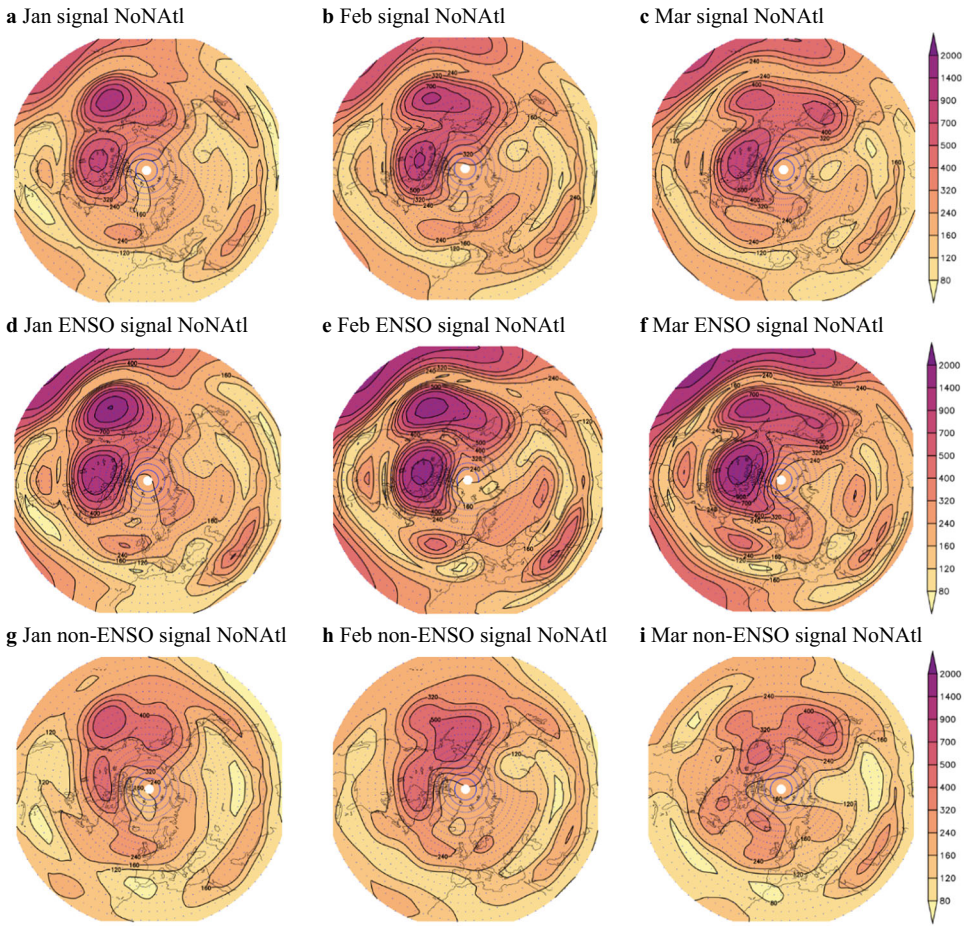


**Fig. 7 January, February, and March signal of geopotential heights at 200 hPa [m$^2$]** in the ICTP AGCM experiment with SST boundary forcing prescribed outside of North Atlantic **(30°–70° N, 80° W–10° E; NoNAtl). a**–**c** The whole 156-year-long period, **d**, **e** ENSO years and **g**–**i** non-ENSO years. Blue dots indicate centres of gridboxes with values larger than the Clim signal. ENSO (53) and non-ENSO events (57) were selected from the 156 years according to the strength of the JFM Niño3.4 index based on NOAA ERSST V3 SST anomalies (ENSO: $|N3.4| > 1\sigma$; non-ENSO: $-0.5\sigma < |N3.4| < 0.5\sigma$).

North Atlantic, we draw attention to the fact that the results for VarGH500 also show a subtle difference over the North Atlantic between the NoNatl and Glob experiments. Therefore, here we consider the connection between the NAE signal and the SST in more detail for both El Niño and La Niña phases (Fig. 10). The first three panels (Fig. 10a–c) show the temporal development of the relationship between GH200 anomalies averaged over the NAEmax region and SSTs, and the following is depicted: (i) positive GH200 anomalies over the NAE region are associated with La Niña conditions; (ii) area of correlations of the same sign extends from the tropical Pacific to the tropical Atlantic in the belt up to about 20° N (enabling the indirect influence of the tropical Pacific that is found in the TroAtl experiment); (iii) tripolar field of correlations in the extratropical North Atlantic, of which the most pronounced positive anomalies are in the belt around 40 – 50° N. In the context of the NAE region, the most interesting area is the one north of 30° N because there is no SST forcing prescribed there in the NoNAtl experiment (Supplementary Fig. 1f). Composite SST anomalies for El Niño (Fig. 10d–f) highlight the strengthening of positive anomalies centre in the western Atlantic (around 45° W, 50 °N) from January to March. Although less pronounced, the negative anomalies south of the positive centre are also strengthening. The SST response to La Niña events is not symmetric with respect to El Niño. While the El Niño composite has a more pronounced isolated centre of positive anomalies south of Greenland that strengthens from January to March (Fig. 10d–f), the La Niña SST composite (Fig. 10g–i) also has positive SSTA in January south of Greenland. They move southward in February and March when they form an almost continuous band of positive anomalies oriented southwest-northeast along the Atlantic, detached from Greenland by spatially small negative patch of SST anomalies. Such SSTA pattern modulates the meridional SST gradient in the region affecting cyclone development and storm tracks[33].

## DISCUSSION

Our modelling approach based on targeted AGCM simulations with SSTA restricted to different ocean basins (Supplementary Fig. 1), provides insight into the relative roles of different tropical oceans to the GH200 signal over the Northern Hemisphere. Special attention is focused on the North Atlantic-European region, and efforts have been made to isolate the ENSO-related signal from other influences. Instead of focusing solely on the late-winter seasonal averages (as in IHB2023[15]), we examined the monthly output from different ICTP AGCM experiments. Our results confirmed that the signal is strongest in the JFM season, indicating seasonal averaging as an appropriate representation, and this is especially true for the Glob experiment. However, experiments with differently prescribed SST forcing have seasonal development which reveals important details of the relative contribution of individual ocean basins. Thus, to obtain a broad

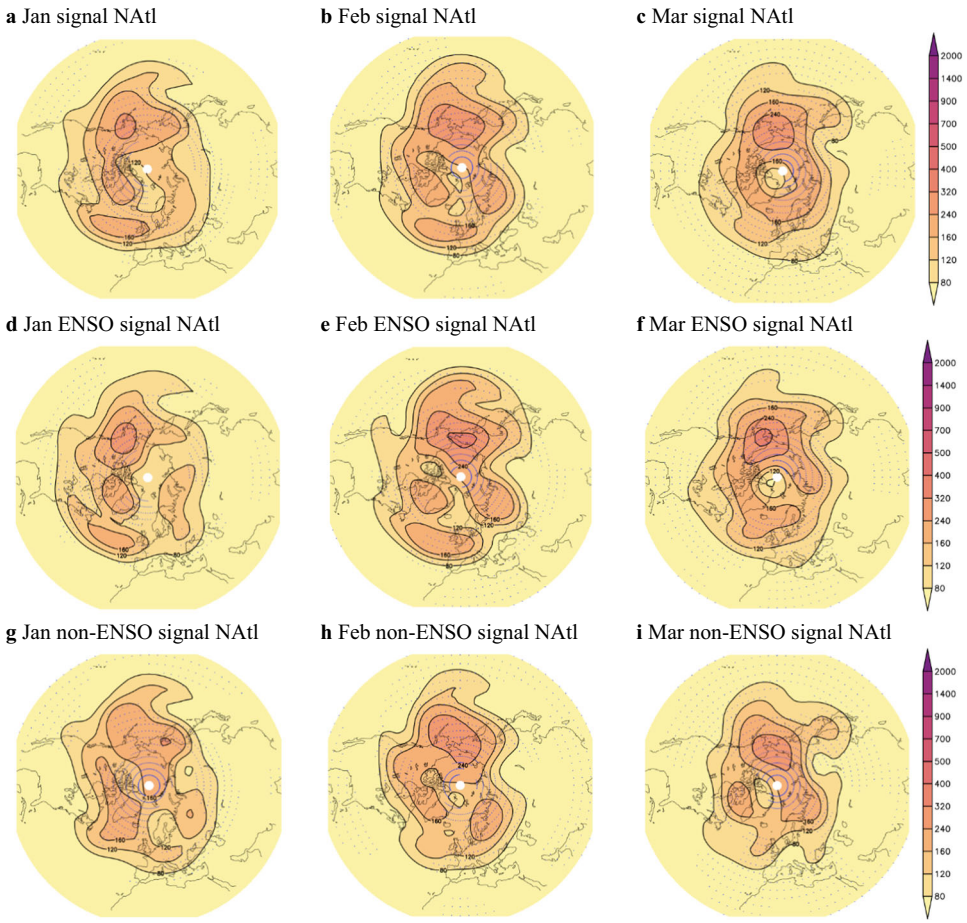


**Fig. 8 January, February, and March signal of geopotential heights at 200 hPa [m$^2$] in the ICTP AGCM experiment with SST boundary forcing prescribed only in North Atlantic (30° N–70° N, 80° W–10° E; NAtl). a–c** The whole 156-year-long period, **d**, **e** ENSO years, and **g–i** non-ENSO years. Blue dots indicate centres of gridboxes with values larger than the Clim signal. ENSO (53) and non-ENSO (57) events were selected from the 156 years according to the strength of the JFM Niño3.4 index based on NOAA ERSST V3 SST anomalies (ENSO: $|N3.4| > 1\sigma$; non-ENSO: $-0.5\sigma < |N3.4| < 0.5\sigma$).

view of the wintertime ENSO impact on the NAE region, it is sufficient to look at the seasonal (JFM) figures. However, for a comprehensive examination related to the relative contribution of different ocean basins, the local influence of North Atlantic SSTs and the two-way sea-atmosphere interaction, a monthly representation is needed because seasonal averaging blurs the important details.

Although the focus of this paper is on the influence of tropical SSTs on the NAE area, we will discuss it here in the context of the entire extratropical response of the Northern Hemisphere. As expected and coinciding with existing literature, the strongest signal is detected over the PNA region during late winter. The signal significantly depends on the experimental design (i.e., SST forcing) with the strongest response found in the Glob, TroPac and Tropics experiments (Fig. 1 and Supplementary Fig. 2), and the signal considering only ENSO years proved to be stronger than its counterpart based on all years (Fig. 2). The non-ENSO signal retains a similar spatial distribution, but is considerably weaker (Fig. 3). The existence of the non-ENSO signal and its strengthening associated with ENSO forcing is consistent with the findings of Molteni et al.[34]. and Palmer[35] who indicated that the PNA extratropical response to SST-forcing projects onto a pre-existing weather regime. Following the approach of Lorenz[36,37], Molteni et al.[34]. explained the midlatitude atmospheric response to tropical SSTs as a 'result of a partial locking of the chaotic extratropical circulation into one of its regimes (regimes which may exist independently from the SST anomalies)'.

In addition to the PNA signal, we also found an ENSO-related signal over the NAE area. The signal appears in the form of a prominent monopole pattern over the North Atlantic (Fig. 2). Although weaker in amplitude, the NAE signal still shows certain similarities with its PNA counterpart. First, both signals are strongest during late winter (Fig. 4). This seasonality is conditioned by the seasonality of ENSO that peaks in winter, and ENSO has been shown to contribute significantly to both PNA and NAE signals. Furthermore, tropical-extratropical teleconnections are established by the propagation of Rossby waves that are SST-excited in the tropics, and the most favourable conditions for their propagation toward the midlatitudes are in winter. In addition to the winter maximum, the NAE signal shows a secondary summer maximum (in June) reflecting the influence of summer ENSO, as shown by Martija-Díez et al.[29]. Second, the signal calculated for ENSO (non-ENSO) years yields a stronger (weaker) atmospheric response over the PNA and NAE regions, which confirms the considerable contribution of the ENSO forcing to the extratropical signal. Third, a very weak signal appears in the experiment without SST forcing (Clim). As already mentioned in the discussion of Supplementary Fig. 2, the Clim signal is a numerical residual resulting from internal atmospheric variability that exists independently of the SST forcing. A weak signal over the same area also appears in the TroAtl and TroInd

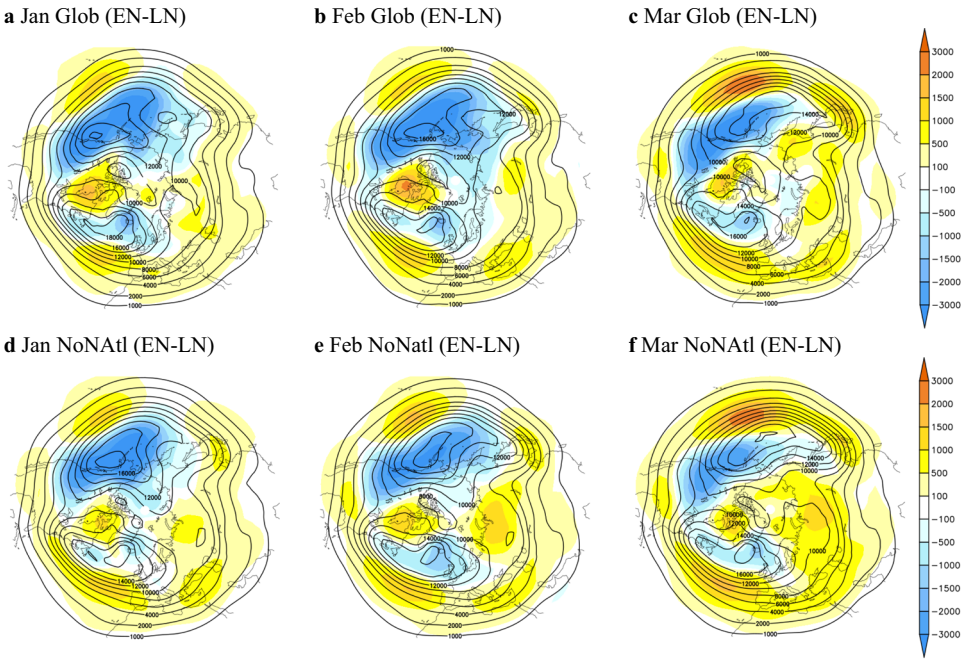


**Fig. 9 January, February, and March difference between the variance of geopotential heights at 500 hPa (GH500) [m$^2$] averaged over El Niño (EN) years (28) and La Niña (LN) years (25) (shading), and GH500 variance averaged over all years (contours). a–c** Glob, and **d–f** NoNAtl ICTP AGCM experiments. El Niño and La Niña years were chosen by the strength of the JFM Niño3.4 index (El Niño: *N*3.4 > 1σ; La Niña: *N*3.4 < −1σ).

experiments. On the other hand, in the ensembles involving SST forcing in the tropical Pacific, the signal is noticeably strengthened (particularly, Glob and TroPac; Supplementary Fig. 2). In addition, a competition between the influence of individual parts of tropical basins is visible in that the experiment with SST forcing constrained to the tropical Pacific produces a stronger signal than the experiment with forcing in the entire tropical belt (cf. Supplementary Fig. 2j–l, m–o).

A separate inspection of the total, ENSO and non-ENSO signals reveals responses projecting onto the same spatial pattern (monopole over the North Atlantic and a tripole over the PNA), but with different amplitudes (cf. Figs. 2, 3, Supplementary Fig. 2). Over both the PNA and NAE regions, the strongest signals are obtained for ENSO years (Fig. 4b, e). In summary, these results demonstrate that a weak NAE signal exists independently of SSTA but is enhanced by SST forcing in the tropical Pacific and this forcing is associated with ENSO events.

Considering these results in the context of the explanation given by Molteni et al.[34]. for the SST-forced response over the PNA, the signal over the NAE region may be analogously considered as atmospheric locking into an existing atmospheric circulation regime. In the case of the PNA region, that is the PNA or TNH pattern defined by Barnston and Livezey[38], with the changing relationship between ENSO and these two response patterns[39]. What is, then, the potential pattern associated with the response over the NAE region? It is well known that the dominant pattern of observed extratropical winter atmospheric circulation over the NAE region is the NAO, which manifests as a leading mode in the empirical orthogonal functions (EOF) analysis, and the model used here can realistically reproduce (IHB2023[15]). As already mentioned in the *Introduction*, it is widely accepted that the ENSO signature over the NAE region is NAO-like. However, our results indicate a monopole pattern of the ENSO-related signal, not the NAO. Thus, if we accept the assumption that the signal is projected onto a pre-existing atmospheric regime, we need to look for a field with a similar action centre over the Atlantic.

According to the findings of IHB2023[15], the first mode of modelled GH200 variability is the NAO, and the EOF2 mode in the NAE region resembles the EA pattern[40–42] (Figs. 2 and 3 in IHB2023[15]). The manifestation of that pattern obtained by EOF analysis is still debated, and descriptions somewhat differ. Thus, some describe it as a north-south dipole extending across the North Atlantic (often referred to as a southward shifted NAO pattern), while other descriptions emphasise a monopole field south of Iceland and west of Ireland[41,43–46]. Regardless, the main action centre of the EA pattern extends along the nodal line of the NAO. Furthermore, according to the findings of IHB2023[15], when the EOF analysis is applied to individual simulations (i.e., ensemble members), the EA pattern is reflected in the *second* EOF for all considered experiments (regardless of the SST forcing; Fig. 3 in IHB2023[15]). On the other hand, when EOF analysis is applied to the ensemble mean, the EA pattern appears as the *first* EOF mode, but only in the SST-forced experiments (see Fig. 2 in IHB2023[15]). The IHB2023[15] results suggest that the SST forcing in the tropical Pacific is essential to obtain the EA pattern as EOF1 (in the ensemble mean of numerical simulations) or as EOF2 (when all individual realisations are considered).

According to the work of Straus and Shukla[47], Barreiro et al.[48], Molteni[49] and Arizmendi et al.[50], the use of ensembles of AGCM simulations forced with SSTs enables the distinction of the internal part of atmospheric variability (resulting from intrinsic dynamics) and the external part (i.e., the SST-forced part); with ensemble mean reflecting the SST-forced component, and individual realisations reflecting the internal variability[51]. In our experiments, the GH200 signal appears as a prominent monopole over the North Atlantic that exists independently of SST forcing (Clim) but is reinforced in SST-forced experiments due to ENSO (Glob, TroPac, and Tropics experiments). Furthermore, this wintertime ENSO-related signal has the spatial structure of the EA mode (cf. Figs. 1, 2 and Supplementary Fig. 2 with EA mode in Fig. 1 of Comas-Bru and Hernández[42]). The AGCM results indicate that the ENSO-related signal projects onto the EA pattern. This is supported by Fig. 6, which shows that a similar pattern of atmospheric response

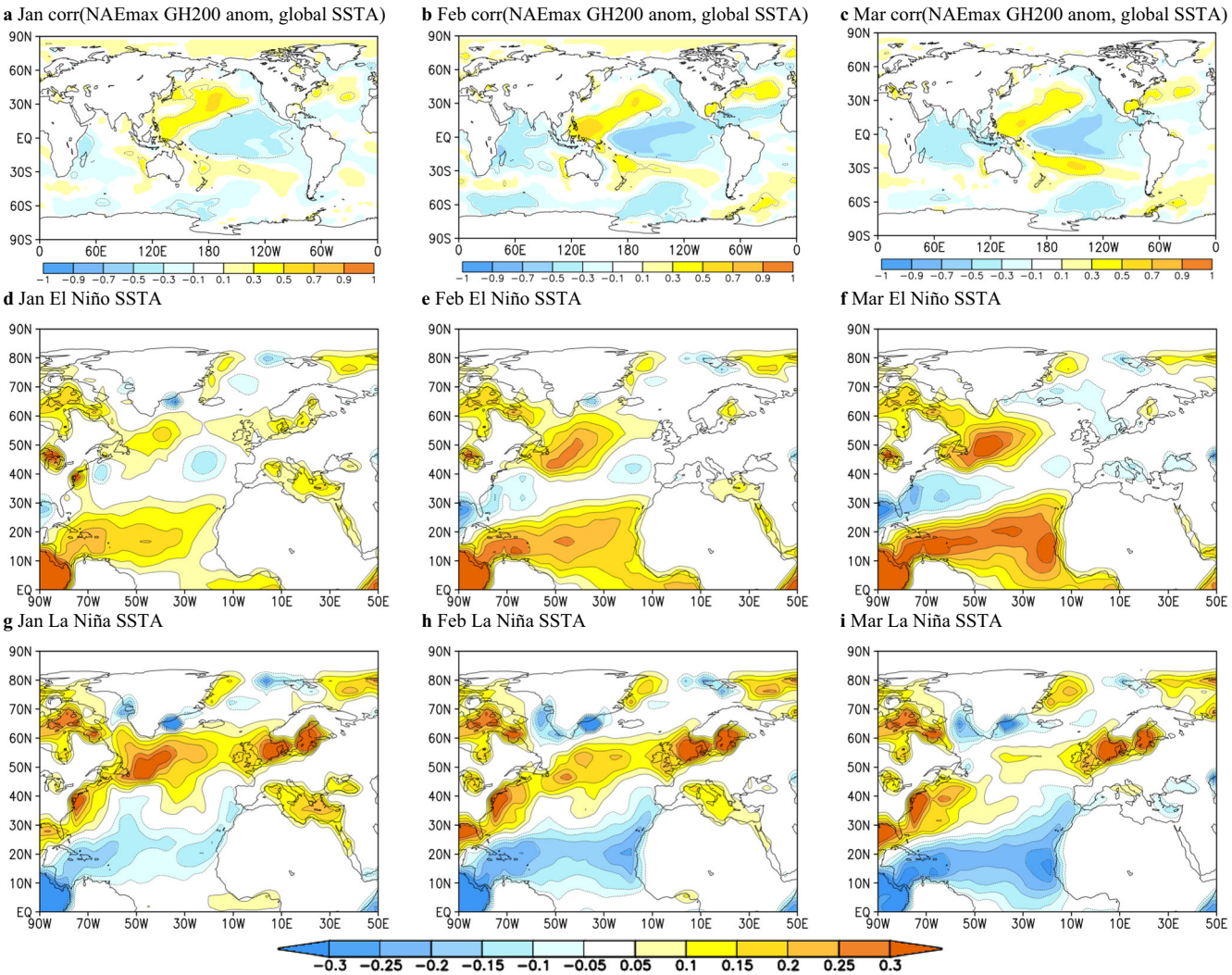


**Fig. 10 Correlations of global NOAA SST anomalies and anomalies of geopotential heights at 200 hPa (GH200) from the ICTP AGCM Glob experiment averaged over the North Atlantic maximum (NAE max; 40°–60° N, 50°–10° W) in 53 ENSO years. a** January, **b** February, and **c** March. The 53 ENSO years were selected from the 156 years according to the strength of the Niño3.4 index in the JFM season ($|N3.4| > 1\sigma$). All statistically significant values based on the two-tailed Student's t test on the 95% confidence level are encircled by dashed contours. January, February, and March composites of SST anomalies (SSTA) [K] in the Atlantic for **d**–**f** El Niño years (28), and **g**–**i** La Niña years (25). El Niño and La Niña years were selected according to the strength of the Niño3.4 index in the JFM season (El Niño: $N3.4 > 1\sigma$; La Niña: $N3.4 < -1\sigma$).

to ENSO is also obtained for the 20CRV3 reanalysis data when the internal variability (NAO) is removed. Even though the magnitudes of the reanalysis are not directly comparable to the signal based on the numerical simulations, the similarity of the spatial pattern, especially in ENSO years, gives us a certain amount of confidence in the ICTP AGCM results and derived conclusions. Furthermore, our results of the atmospheric response projecting onto the EA pattern are consistent with the recent findings of King et al.[52]. who identified a non-NAO part of ENSO-related teleconnections over the NAE region.

The relative ratio of the signal amplitude experiments with differently prescribed SST forcing indicates the possible existence of a signal-amplifying process outside the tropical Pacific. Additional AGCM experiments (NoNAtl and NAtl) point to the extratropical North Atlantic as a contributing factor. Although the atmospheric response to midlatitude SST forcing is weak, extratropical air-sea interaction still can be an important modifier of local atmospheric variability. Previous studies by Herceg-Bulic and Kucharski[23,53] and Herceg-Bulic et al.[24]. have already suggested the role of extratropical air-sea coupled processes for the delayed impact of ENSO on the NAE region. Thus, SST anomalies in the North Atlantic act as a physical link between the winter ENSO forcing and atmospheric variability in the following spring, as well as a contributing factor to the seasonal persistence of the NAO[23,24,53]. The basic physical mechanism involves atmospheric anomalies that serve as an 'atmospheric bridge' through which the influence of ENSO-related SST anomalies is transferred remotely to the midaltitude Atlantic creating an SST pattern that can reinforce the local atmospheric circulation that has driven them[32]. The persistence of this SST pattern in the North Atlantic enables the prolonged influence of ENSO and NAO[17]. Additionally, we have found that both, tropical and extratropical SSTs affect storm tracks and GH200 signal over the NAE region. ENSO-related impact on the North Atlantic manifests in a latitudinal shift of storm tracks (Fig. 9).

In addition, local North Atlantic SSTs also play a role. We have demonstrated a two-way nature of this atmosphere-ocean interaction: ENSO-related atmospheric circulation induces the

SST pattern in the North Atlantic (Fig. 10) that further modulates the meridional SST gradient and local surface baroclinity which ultimately affects the storm tracks[27]. El Niño events are associated with an SST pattern in the extratropical North Atlantic that smooths the SST gradient yielding reduced cyclone activity and supporting a southward shift of the storm tracks, which has been already initiated with the remote influence of El Niño. Considering the relatively small effect of extratropical SSTs compared to the stronger tropical SST influence, their influence is not prevailing, but is still detectable and affects the local features of the ENSO signature. To capture certain details of the influence of midlatitude SSTs it is necessary to consider this influence separately for El Niño and La Niña because they are not symmetric. Although the La Niña SST pattern is different from the El Niño one, there are warm SSTs along the eastern North American coast in both patterns. Here, we hypothesise that such an SST pattern can smooth the SST gradient in the same manner as discussed for El Niño. Then, the reduced meridional SST gradient would have a similar impact on the overlaying atmosphere as during El Niño events (suppressed cyclonic activity and equatorward shift of storm tracks). In this case, the remote La Niña impact and the effect of extratropical North Atlantic SSTs on storm tracks would be opposite, yielding a weaker response. Such interplay between remote and local SST impact could be a partial cause of the weaker atmospheric response to La Niña than to El Niño of the same amplitude which has been reported in some studies (e.g. refs. [3,13]). The ENSO-extratropical Atlantic SSTs interaction and impact on GH200 signal over the NAE region through the modulation of storm tracks definitively warrants further investigation with a detailed analysis of the two-way atmosphere-ocean interaction and related momentum, moisture and heat transports based on carefully designed experimentation, including the use of coupled ocean-atmosphere models and the analysis of observations.

In summary, in this paper, we discussed the signal of geopotential heights at 200 hPa over the North Atlantic-European region from the perspective of its seasonality, the contribution of different tropical basins, ENSO impact, spatial pattern, linearity of the atmospheric response, the contribution of storm tracks, two-way atmosphere-ocean interaction over the extratropical Atlantic and superposition of remote (ENSO) and local (midlatitude North Atlantic) SST impact. Our study once again demonstrates the complexity of extratropical atmospheric circulation. The response to ENSO is also noticeable in the NAE area, but it is not easy to disentangle the ENSO-related signal from other influences. It is challenging to isolate and understand the processes that define the ENSO signature under conditions of competitive interaction of tropical basins, regional atmosphere-ocean interaction, the impact of local SSTs, modulation of storm tracks and internal atmospheric variability with the dominant influence of the NAO.

The strongest signal is detected in the late-winter months. Using an intermediately complex atmospheric general circulation model (ICTP AGCM), we designed targeted experiments with differently prescribed SSTA that act as a source of lower boundary forcing. The results of the Glob experiment forced with global SSTA have shown that the NAE signal has a distinctive centre of action above the North Atlantic. For both the modelled signal and 20CRV3 variance, ENSO dependence of the NAE signal is demonstrated. Thus, the North Atlantic maximum expands if only ENSO years are considered. However, the signal with the same spatial pattern also exists in non-ENSO years but is less pronounced. Moreover, it exists also in the unforced experiment (Clim) and experiments without SST forcing in the tropical Pacific (TroAtl and TroInd), but with a much weaker amplitude. The results presented in this paper indicate that the NAE atmospheric response to ENSO forcing can be viewed similarly to what Molteni et al.[34]. proposed for the response over the PNA - locking of the chaotic extratropical circulation into one of its regimes. In this way, ENSO-forced signal over the NAE region also projects onto an existing atmospheric regime. Here, that regime is the East Atlantic pattern.

The experimental design made it possible to assess the relative contributions of individual parts of tropical basins. The contribution of the tropical Pacific (ENSO) turned out to be the most significant. Furthermore, the signal obtained in the experiment with SST forcing in the entire tropical belt is not a simple sum of the signals obtained in individual SST-forced experiments. Rather, a competitive interaction between the influences of individual tropical basins is indicated.

In the NAE region, atmospheric circulation linked to ENSO events drives an SST pattern in the extratropical North Atlantic which is shown to act as a modifier of the NAE ENSO-related signal through a two-way atmosphere-ocean interaction. Extratropical North Atlantic SSTs influence the pre-existing ENSO-induced atmospheric circulation by modulating cyclonic activity and storm tracks. However, the local SST effect is weaker than the one associated with ENSO, but still important for the local details of the ENSO signal over the NAE region. In addition, the extratropical North Atlantic SST response to ENSO-related atmospheric forcing is not symmetric for El Niño and La Niña events. Namely, due to the specificity of the SST anomalies pattern generated in the North Atlantic during El Niño and La Niña events, there may be a constructive superposition of the local influence of SST on storm tracks with the remote SST influence of the tropical Pacific (amplification of the GH200 signal) for El Niño events, while the superposition is destructive for La Niña (attenuation of the GH200 signal). Thus, the extratropical Atlantic SSTs are a possible contributor to the nonlinearity of the atmospheric response to El Niño and La Niña events. From this point of view, tropical SSTs are strong generators of global climate variability, but local extratropical SSTs, despite their slight impact, are important factors that give a special flavour to the atmospheric response to remote SST forcing.

## METHODS

### Model description

In this study, we used the International Centre for Theoretical Physics (ICTP) general circulation model of the atmosphere (ICTP AGCM; SPEEDY). ICTP AGCM is a model of intermediate complexity with spectral triangular truncation at wavenumber 30 (T30) and eight vertical levels[49,54,55]. The base of the model consists of a hydrostatic spectral dynamical core from the Geophysical Fluid Dynamics Laboratory[56]. ICTP AGCM is a spectral transform model with a vorticity-divergence form, as described by Bourke[57], with the semi-implicit treatment of gravity waves. Also, the model utilises the σ-coordinate. Parametrisation schemes for convection, large-scale condensation, shortwave and longwave radiation, and surface fluxes of heat, moisture, and momentum are all used within the ICTP AGCM. Here, a single layer thermodynamic model is used to calculate land and sea-ice temperature anomalies[55]. The input files for SST and sea-ice climatology are taken from the NOAA ERSST V3[58] and Hadley Centre HADISST datasets[59]. A more detailed description of the model is available at the following link: https://users.ictp.it/~kucharsk/speedy-net.html

Various studies confirm the ability of the ICTP AGCM to successfully simulate the main characteristics of teleconnections with the extratropical region during different seasons (e.g. refs. [23,24,54,60,61]). More recently, Abid et al.[6] showed that the model could even be used for studying subseasonal conditions. Additionally, the model was used to examine the sensitivity of ENSO teleconnections over the Pacific North American region to the mean state of the model[62].

### Experimental design

The seven ICTP AGCM experiments analysed in this study have lower boundary SST forcing limited to different ocean areas, while

the remaining oceans contain only climatological SST values. This lower boundary forcing is based on monthly NOAA ERSST V3 SSTA[58]. The Glob experiment has observed SSTA prescribed globally (90° S to 90° N, 0°–360° E), while the Tropics experiment has the boundary forcing applied in the entire tropical zone (30° S to 30° N, 0°−360° E). The boundary forcing in the TroAtl experiment is limited to the tropical Atlantic area (30° S to 30° N, 100° W to 20° E), while the TroInd experiment has the prescribed forcing only in the tropical Indian Ocean (30° S to 30° N, 30°−120° E). The simulations in the TroPac experiment are forced by SSTA in the tropical Pacific (30° S to 30° N, 120° E to 60° W). To analyse the separate impact of the extratropical North Atlantic, the NoNAtl experiment has SST forcing prescribed everywhere except in the extratropical North Atlantic (Supplementary Fig. 1f), while the Natl experiment is forced with SST anomalies constrained to the North Atlantic (Natl; 30° S to 30° N, 80° W to 10° E; Supplementary Fig. 1g). Additionally, the results of an experiment without any boundary forcing (i.e., containing only climatological SSTs; Clim) are analysed. Such experimental design enables the separation of influences of individual basins and the estimation of their relative contribution to the total signal. To illustrate the areas in which SST boundary forcing is applied in the previously described AGCM experiments, monthly-varying SSTA for January 2010 are displayed in Supplementary Fig. 1. The Clim experiment is not shown because there is no SSTA prescribed in its design.

All AGCM experiments consist of a 35-member ensemble of 156-year-long numerical simulations. The ensemble members within each experiment have identically prescribed SST boundary forcing and differ only in initial conditions set by varying lengths of the random diabatic forcing within the first year of model integration. The AGCM experiments were conducted between 1854 and 2010, where the first year is not further considered in the analysis.

### Signal variance analysis

The signal analysed within this study is defined by the difference between the ensemble mean and the climatological mean of each AGCM experiment for the whole 156-year considered period. Following Branković and Molteni[63] and Chapman et al.[30], the signal definition, for any variable $x$, is given in Eq. (1),

$$\sigma_s^2 = \frac{1}{N}\sum_{j=1}^{N}\left(\overline{x}_j - \overline{x}\right)^2, \quad (1)$$

where $\overline{x}_j = \sum_i^M x_{ij}$ is the ensemble mean for the $j$th year, $x_{ij}$ is the $i$th ensemble member in the $j$th year, $\overline{x}$ is the ensemble mean average across all $N$ years (i.e., the climatological mean of the ensemble mean), $N$ represents the number of years, and $M$ is the number of ensemble members. Before calculating the signal, all data were linearly detrended and a high-pass filter (keeping periods only shorter than 11 years) was applied to reveal the interannual variability that is of interest for this study.

The signal is calculated for all years, then ENSO and non-ENSO years, respectively, to detect the extent of the ENSO influence on the monthly signal of geopotential heights at 200 hPa (GH200) over the North Atlantic-European region (NAE; 30°−60° N, 50° W to 30° E). According to the value of the late-winter Niño3.4 index (January, February, March; JFM), 53 of 156 years are categorised as ENSO years ($|N3.4|>1.0\sigma$), while 57 years are labelled non-ENSO years ($-0.5\sigma<N3.4<0.5\sigma$). Here, the Niño3.4 index is defined by NOAA ERSST V3 SST anomalies[58] averaged over the area: 5° S to 5° N, 120°−170° W.

## DATA AVAILABILITY

NOAA-CIRES-DOE 20th Century Reanalysis (V3) data are available at https://psl.noaa.gov/data/gridded/data.20thC_ReanV3.html. NOAA ERSST V3 SST data are available at https://psl.noaa.gov/data/gridded/data.noaa.ersst.v3.html. All relevant data are available from the corresponding author upon reasonable request.

## CODE AVAILABILITY

The codes for the analysis of this study are available from the corresponding author upon reasonable request. The code of ICTPAGCM is available through the URL: https://www.ictp.it/research/esp/models/speedy.aspx.

Received: 15 February 2023; Accepted: 6 October 2023;
Published online: 26 October 2023

## REFERENCES

1. Domeisen, D. I. V., Garfinkel, C. I. & Butler, A. H. The teleconnection of El Niño Southern oscillation to the stratosphere. *Rev. Geophys.* **57**, 5–47 (2019).
2. Ineson, S. & Scaife, A. A. The role of the stratosphere in the European climate response to El Niño. *Nat. Geosci.* **2**, 32–36 (2009).
3. Jiménez-Esteve, B. & Domeisen, D. I. V. The tropospheric pathway of the ENSO–North Atlantic teleconnection. *J. Clim.* **31**, 4563–4584 (2018).
4. Mezzina, B. et al. Multi-model assessment of the late-winter extra-tropical response to El Niño and La Niña. *Clim. Dyn.* https://doi.org/10.1007/s00382-020-05415-y (2020).
5. Mezzina, B. et al. Multi-model assessment of the late-winter stratospheric response to El Niño and La Niña. *Clim. Dyn.* https://doi.org/10.1007/s00382-021-05836-3 (2021).
6. Abid, M. A. et al. Separating the Indian and Pacific Ocean impacts on the Euro-Atlantic response to ENSO and its transition from early to late winter. *J. Clim.* 1–57 https://doi.org/10.1175/jcli-d-20-0075.1 (2020).
7. Ayarzagüena, B., Ineson, S., Dunstone, N. J., Baldwin, M. P. & Scaife, A. A. Intra-seasonal effects of El Niño-Southern Oscillation on North Atlantic climate. *J. Clim.* **31**, 8861–8873 (2018).
8. Joshi, M. K., Abid, M. A. & Kucharski, F. The role of an Indian Ocean heating dipole in the ENSO teleconnection to the North Atlantic European region in early winter during the twentieth century in reanalysis and CMIP5 Simulations. *J. Clim.* **34**, 1047–1060 (2021).
9. King, M. P. et al. Importance of late fall ENSO teleconnection in the Euro-Atlantic sector. *Bull. Am. Meteorol. Soc.* **99**, 1337–1343 (2018).
10. King, M. P., Li, C. & Sobolowski, S. Resampling of ENSO teleconnections: accounting for cold-season evolution reduces uncertainty in the North Atlantic. *Weather Clim. Dyn.* **2**, 759 (2021).
11. Huang, J., Higuchi, K. & Shabbar, A. The relationship between the North Atlantic Oscillation and El Niño-Southern Oscillation. *Geophys. Res. Lett.* **25**, 2707–2710 (1998).
12. Pinto, J. G., Reyers, M. & Ulbrich, U. The variable link between PNA and NAO in observations and in multi-century CGCM simulations. *Clim. Dyn.* **36**, 337–354 (2011).
13. Brönnimann, S. Impact of El Niño-Southern Oscillation on European climate. *Rev. Geophys.* **45**, RG3003 (2007).
14. Hurrell, J. W., Kushnir, Y., Ottersen, G. & Visbeck, M. An overview of the North Atlantic Oscillation. *Geophys. Monogr. Ser.* **134**, 1–35 (2003).
15. Ivasić, S. & Herceg-Bulić, I. A modelling study of the impact of tropical SSTs on the variability and predictable components of seasonal atmospheric circulation in the North Atlantic–European region. *Clim. Dyn.* **60**, 927–944 (2023).
16. Lopez, H. & Kirtman, B. P. ENSO influence over the Pacific North American sector: uncertainty due to atmospheric internal variability. *Clim. Dyn.* **52**, 6149–6172 (2019).
17. Sutton, R. T. & Hodson, D. L. R. Influence of the ocean on North Atlantic climate variability 1871-1999. *J. Clim.* **16**, 3296–3313 (2003).
18. Terray, L. & Cassou, C. Tropical Atlantic sea surface temperature forcing of quasi-decadal climate variability over the North Atlantic-European region. *J. Clim.* **15**, 3170–3187 (2002).
19. Venzke, S., Allen, M. R., Sutton, R. T. & Rowell, D. P. The atmospheric response over the North Atlantic to decadal changes in sea surface temperature. *J. Clim.* **12**, 2562–2584 (1999).
20. Lau, N. C. & Nath, M. J. A modeling study of the relative roles of tropical and extratropical SST anomalies in the variability of the global atmosphere-ocean system. *J. Clim.* **7**, 1184–1207 (1994).
21. Lau, N. C. & Nath, M. J. The role of the 'atmospheric bridge' in linking tropical pacific ENSO events to extratropical SST anomalies. *J. Clim.* **9**, 2036–2057 (1996).
22. Lau, N. C. & Nath, M. J. Impact of ENSO on SST variability in the North Pacific and North Atlantic: Seasonal dependence and role of extratropical sea-air coupling. *J. Clim.* **14**, 2846–2866 (2001).
23. Herceg-Bulić, I. & Kucharski, F. Delayed ENSO impact on spring precipitation over North/Atlantic European region. *Clim. Dyn.* **38**, 2593–2612 (2012).
24. Herceg-Bulić, I., Mezzina, B., Kucharski, F., Ruggieri, P. & King, M. P. Wintertime ENSO influence on late spring European climate: the stratospheric response and the role of North Atlantic SST. *Int. J. Climatol.* **37**, 87–108 (2017).

25. James, I. N. & Burkhardt, U. A sidelong look at storm tracks. *Atmos. Sci. Lett.* **7**, 69–74 (2006).
26. Li, Y. & Lau, N. C. Contributions of downstream Eddy development to the teleconnection between ENSO and the atmospheric circulation over the North Atlantic. *J. Clim.* **25**, 4993–5010 (2012).
27. Nakamura, H., Sampe, T., Tanimoto, Y. & Shimpo, A. Observed associations among storm tracks, jet streams and midlatitude oceanic fronts. *Geophys. Monogr. Ser.* **147**, 329–345 (2004).
28. Ciasto, L. M., Li, C., Wettstein, J. J. & Kvamstø, N. G. North Atlantic storm-track sensitivity to projected sea surface temperature: Local versus remote influences. *J. Clim.* **29**, 6973–6991 (2016).
29. Martija-Díez, M., López-Parages, J., Rodríguez-Fonseca, B. & Losada, T. The stationarity of the ENSO teleconnection in European summer rainfall. *Clim. Dyn.* https://doi.org/10.1007/S00382-022-06596-4 (2022).
30. Chapman, W. E. et al. Monthly modulations of ENSO teleconnections: Implications for potential predictability in North America. *J. Clim.* **34**, 5899–5921 (2021).
31. Slivinski, L. C. et al. Towards a more reliable historical reanalysis: Improvements for version 3 of the Twentieth Century Reanalysis system. *Q. J. R. Meteorol. Soc.* **145**, 2876–2908 (2019).
32. Kushnir, Y. et al. Atmospheric GCM response to extratropical SST anomalies: synthesis and evaluation. *J. Clim.* **15**, 2233–2256 (2002).
33. Tsopouridis, L., Spengler, T. & Spensberger, C. Smoother versus sharper Gulf Stream and Kuroshio sea surface temperature fronts: effects on cyclones and climatology. *Weather Clim. Dyn.* **2**, 953–970 (2021).
34. Molteni, F., Ferranti, L., Palmer, T. N. & Viterbo, P. A dynamical interpretation of the global response to equatorial Pacific SST anomalies. *J. Clim.* **6**, 777–795 (1993).
35. Palmer, T. N. Extended-range atmospheric prediction and the Lorenz model. *Bull. Am. Meteorol. Soc.* **74**, 49–65 (1993).
36. Lorenz, E. N. Deterministic nonperiodic flow. *J. Atmos. Sci.* **20**, 130–141 (1963).
37. Lorenz, E. N. Can chaos and intransitivity lead to interannual variability? *Tellus A* **42**, 378–389 (1990).
38. Barnston, A. G. & Livezey, R. E. Classification, seasonality and persistence of low-frequency atmospheric circulation patterns. *Mon. Weather Rev.* **115**, 1083–1126 (1987).
39. Soulard, N., Lin, H. & Yu, B. The changing relationship between ENSO and its extratropical response patterns. *Sci. Rep.* **9**, 6507 (2019).
40. Moore, G. W. K., Renfrew, I. A. & Pickart, R. S. Multidecadal mobility of the North Atlantic oscillation. *J. Clim.* **26**, 2453–2466 (2013).
41. Comas-Bru, L. & Mcdermott, F. Impacts of the EA and SCA patterns on the European twentieth century NAO-winter climate relationship. *Q. J. R. Meteorol. Soc.* **140**, 354–363 (2014).
42. Comas-Bru, L. & Hernández, A. Reconciling North Atlantic climate modes: revised monthly indices for the East Atlantic and the Scandinavian patterns beyond the 20th century. *Earth Syst. Sci. Data* **10**, 2329–2344 (2018).
43. Bastos, A. et al. European land CO2 sink influenced by NAO and East-Atlantic Pattern coupling. *Nat. Commun.* **7**, 10315 (2016).
44. Chafik, L., Nilsen, J. E. Ø. & Dangendorf, S. Impact of North Atlantic teleconnection patterns on northern European sea level. *J. Mar. Sci. Eng.* **5**, 43 (2017).
45. Moore, G. W. K. & Renfrew, I. A. Cold European winters: Interplay between the NAO and the East Atlantic mode. *Atmos. Sci. Lett.* **13**, 1–8 (2012).
46. Zubiate, L., McDermott, F., Sweeney, C. & O'Malley, M. Spatial variability in winter NAO–wind speed relationships in western Europe linked to concomitant states of the East Atlantic and Scandinavian patterns. *Q. J. R. Meteorol. Soc.* **143**, 552–562 (2017).
47. Straus, D. M. & Shukla, J. Distinguishing between the SST-forced variability and internal variability in mid latitudes: analysis of observations and GCM simulations. *Q. J. R. Meteorol. Soc.* **126**, 2323–2350 (2000).
48. Barreiro, M., Chang, P. & Saravanan, R. Variability of the South Atlantic convergence zone simulated by an atmospheric general circulation model. *J. Clim.* **15**, 745–763 (2002).
49. Molteni, F. Atmospheric simulations using a GCM with simplified physical parametrizations. I: model climatology and variability in multi-decadal experiments. *Clim. Dyn.* **20**, 175–191 (2003).
50. Arizmendi, F., Martí, A. C. & Barreiro, M. Evolution of atmospheric connectivity in the 20th century. *Nonlinear Process. Geophys.* **21**, 825–839 (2014).
51. Straus, D. M. & Shukla, J. Does ENSO force the PNA? *J. Clim.* **15**, 2340–2358 (2002).
52. King, M. P., Keenlyside, Noel & Li, C. ENSO teleconnections in terms of non-NAO and NAO atmospheric variability. *Clim. Dyn.* **1**, 1–17 (2023).
53. Herceg-Bulić, I. & Kucharski, F. North Atlantic SSTs as a link between the wintertime NAO and the following spring climate. *J. Clim.* **27**, 186–201 (2014).
54. Kucharski, F., Molteni, F. & Bracco, A. Decadal interactions between the western tropical Pacific and the North Atlantic Oscillation. *Clim. Dyn.* **26**, 79–91 (2006).
55. Kucharski, F. et al. On the need of intermediate complexity general circulation models: A "sPEEDY" example. *Bull. Am. Meteorol. Soc.* **94**, 25–30 (2013).
56. Held, I. M. & Suarez, M. J. A proposal for the intercomparison of the dynamical cores of atmospheric general circulation models. *Bull. Am. Meteorol. Soc.* **75**, 1825–1830 (1994).
57. Bourke, W. A multi-level spectral model. I. Formulation and hemispheric integrations. *Mon. Weather Rev.* **102**, 687–701 (1974).
58. Smith, T. M., Reynolds, R. W., Peterson, T. C. & Lawrimore, J. Improvements to NOAA's historical merged land-ocean surface temperature analysis (1880-2006). *J. Clim.* **21**, 2283–2296 (2008).
59. Rayner, N. A. et al. Global analyses of sea surface temperature, sea ice, and night marine air temperature since the late nineteenth century. *J. Geophys. Res. Atmos.* https://doi.org/10.1029/2002jd002670 (2003).
60. Dogar, M. M., Kucharski, F. & Azharuddin, S. Study of the global and regional climatic impacts of ENSO magnitude using SPEEDY AGCM. *J. Earth Syst. Sci.* **126**, 30 (2017).
61. Ruggieri, P., Kucharski, F., Buizza, R. & Ambaum, M. H. P. The transient atmospheric response to a reduction of sea-ice cover in the Barents and Kara Seas. *Q. J. R. Meteorol. Soc.* **143**, 1632–1640 (2017).
62. Di Carlo, E., Ruggieri, P., Davini, P., Tibaldi, S. & Corti, S. ENSO teleconnections and atmospheric mean state in idealised simulations. *Clim. Dyn.* **59**, 1–18 (2022).
63. Branković, Č. & Molteni, F. Seasonal climate and variability of the ECMWF ERA-40 model. *Clim. Dyn.* **22**, 139–156 (2004).

## ACKNOWLEDGEMENTS

This work has been supported in part by the Croatian Science Foundation under the project UIP-2017-05-6396 (CroClimGoGreen).

## AUTHOR CONTRIBUTIONS

The study design was proposed by I.H.B. Material preparation, numerical simulations with ICTP AGCM, and data collection were performed by S.I. and I.H.B. Results were visualised by M.P. and S.I. Experimental design, data and methods were written by S.I. Results, discussion and conclusions were written by I.H.B. with help of S.I. All three authors contributed to the data analysis, discussion, interpretation of results, and writing and editing of the manuscript. All authors read and approved the final manuscript.

## COMPETING INTERESTS

The authors declare no competing interests.

## ADDITIONAL INFORMATION

**Supplementary information** The online version contains supplementary material available at https://doi.org/10.1038/s41612-023-00493-1.

**Correspondence** and requests for materials should be addressed to Ivana Herceg-Bulić.